Heliyon 8 (2022) e11274

Contents lists available at ScienceDirect

Heliyon

journal homepage: www.cell.com/heliyon

Research article

Computational studies on thermo-kinetics aspects of pyrolysis of isopropyl acetate and its methyl, bromide and hydroxyl derivatives

S.H. Reza Shojaei [a,b], Abolfazl Shiroudi [c,**], Mohamed A. Abdel-Rahman [d,*]

[a] Department of Physics, Faculty of Science, Sahand University of Technology, Tabriz, 51335-1996, Iran
[b] X-LAB, Hasselt University, Agoralaan, Diepenbeek, 3590, Belgium
[c] Research Club, IQneiform Oy, Juva, Finland
[d] Chemistry Department, Faculty of Science, Suez University, Suez, 43518, Egypt

ARTICLE INFO

Keywords:
Isopropyl acetates
Pyrolysis
Rate coefficients
DFT
NBO
Reaction mechanisms

ABSTRACT

The gas-phase decomposition kinetics of isopropyl acetate (IPA) and its methyl, bromide and hydroxyl derivatives into the corresponding acid and propene were investigated using density functional theory (DFT) with the ωB97XD and M06–2x functionals, as well as the benchmark CBS-QB3 composite method. Transition state theory (TST) and RRKM theory calculations of rate constants under atmospheric pressure and in the fall-off regime were used to supplement the measured energy profiles. The results show that the formation of propene and bromoacetic acid is the most dominant pathway at the CBS-QB3 composite method, both kinetically and thermodynamically. There was a good agreement with experimental results. Pressures greater than 0.01 bar, corresponding to larger barrier heights are insufficient to ensure saturation of the measured rate coefficient when compared to the RRKM kinetic rates.

Natural bond orbitals (NBO) charges, bond orders, bond indices, and synchronicity parameters all point to the considered pathways taking place via a homogenous, first-order concerted, as well as an asynchronous mechanism involving a non-planar cyclic six-membered transition state. The calculated data exhibit that the elongation of the $C_{\alpha}-O$ bond length and subsequent polarization of the $C_{\alpha}^{+\delta}\ldots O^{-\delta}$ bond is the rate-determining step of the considered reactions in the cyclic transition state, which appears to be involved in this type of reaction.

1. Introduction

Ester pyrolysis has received a lot of attention [1, 2, 3, 4]. The corresponding acid and alkene are the products of esters containing a β-hydrogen in the alkyl group. Hurd and Blunk [3] proposed that alkyl esters pyrolysis by simultaneously breaking the O−R bond and forming an O–H bond between the carbonyl oxygen and the hydrogen of the ester's alkyl portion (see Scheme 1). They proposed a mechanism involving a "cyclic hydrogen bridge" to explain the pyrolysis of esters into acid and alkene. Kinetic studies display that this is a first-order homogeneous reaction. All of these point to a mechanism involving a quasi-cyclic intermediate as.

It is reasonable to believe that the ortho-substituents involved may delay the formation of an O–H bond, thereby stabilizing these esters by preventing the formation of the postulated six-membered cyclic intermediate [5].

Many biodiesel models [6, 7, 8, 9] received a lot of attention both theoretically and experimentally. A few experimental and computational studies [10, 11, 12, 13, 14] have been conducted on isopropyl acetate (IPA) and its derivatives. **IPA** as the simplest branched biodiesel ester molecule is commercially produced by esterifying acetic acid and isopropanol and is widely used in the production of fats, oil, plastics, printing inks, perfumes, varnishes, adhesive agents, and synthetic resins [15, 16, 17]. The decomposition of three secondary acetates (isopropyl propionate, isopropyl glycolat, and isopropyl bromoacetate) were measured in a static system at temperatures ranging from 563 to 623 K and pressures ranging from 54 to 250 Torr, as well as isopropyl acetate, has been experimentally studied [18, 19] at pressures ranging from 1.03 to 2.28 mmHg and temperatures ranging from 714.7 to 801 K, indicating positive activation energy. The rate constants of these secondary acetates were discovered to be independent of their initial pressure.

* Corresponding author.
** Corresponding author.
E-mail addresses: shiroudi@gmail.com (A. Shiroudi), Mohamed.Abdel-Rahman@sci.suezuni.edu.eg (M.A. Abdel-Rahman).

https://doi.org/10.1016/j.heliyon.2022.e11274
Received 8 August 2022; Received in revised form 5 October 2022; Accepted 21 October 2022

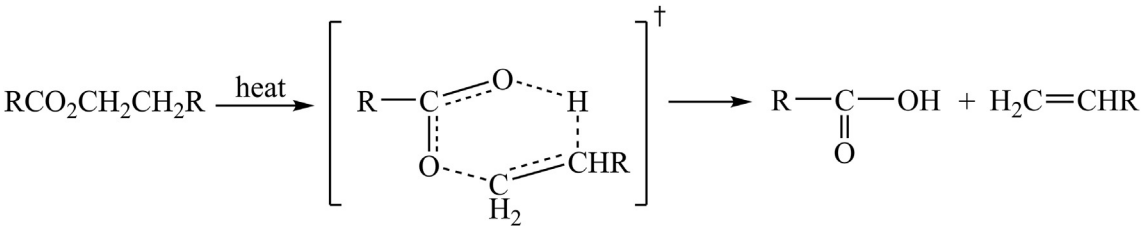

Scheme 1. Pyrolysis mechanism of esters through six-membered cyclic intermediate.

The kinetics of the gas-phase unimolecular pyrolysis of **IPA** and its methyl, bromide and hydroxyl derivatives [X–$CH_2CO_2CHMe_2$ with X = Me, OH, and Br] into $CH_3CH = CH_2$ and X–CH_2COOH were experimentally investigated in a static system at pressures ranging from 54 to 250 Torr and temperatures ranging from 563 to 623 K. Chemical reactions in seasoned vessels are homogeneous, unimolecular, and follow a first-order law [18].

Emovon [20] showed an important relationship between the pyrolysis rate constant of several *tert*-butyl-substituted acetates and the acid's pK_a values, *viz.* $CC1_2 > C1 > H > Me$. Using electronic structure theory, the mechanism of this reaction was interpreted [21] as a six-membered ring transition state in which C–O and C–H bonds are simultaneously broken, followed by olefin formation [22].

Figure 1 depicts an Arrhenius plot of the calculated rate coefficients against the considered temperature ranges. The rate constants of pyrolysis of secondary acetates such as isopropyl acetate (**1**, X = H), isopropyl propionate (**2**, X = Me), isopropyl glycolate (**3**, X = OH), and isopropyl bromoacetate (**4**, X = Br) exhibit positive temperature dependences with activation energies of (−47.5 ± 1.9) (−45.4 ± 0.2) (−43.0 ± 0.7), and (−43.3 ± 1.4) kcal mol^{-1}, respectively [18, 19]. Chuchani *et al.* [18], and Blades [19], demonstrated for the considered reactions, all obtained temperature-dependent rate constants and fitted modified Arrhenius expressions obtained approximately by the least squares procedure were as follows:

$$\log k_1\left(\sec^{-1}\right) = (13.85 \pm 0.02) - \left[\frac{(47.5 \pm 1.9)\ \text{kcal/mol}}{2.303\,RT}\right];$$

$$(T = 440 - 630\ \text{K})$$

$$\log k_2\left(\sec^{-1}\right) = (13.06 \pm 0.09) - \left[\frac{(45.4 \pm 0.2)\ \text{kcal/mol}}{2.303\,RT}\right];$$

$$(T = 583.2 - 624.1\ \text{K})$$

$$\log k_3\left(\sec^{-1}\right) = (12.56 \pm 0.28) - \left[\frac{(43.0 \pm 0.7)\ \text{kcal/mol}}{2.303\,RT}\right];$$

$$(T = 573.2 - 623.1\ \text{K})$$

$$\log k_4\left(\sec^{-1}\right) = (12.84 \pm 0.02) - \left[\frac{(43.3 \pm 1.4)\ \text{kcal/mol}}{2.303\,RT}\right];$$

$$(T = 563.5 - 623.1\ \text{K})$$

In the considered temperature ranges, the Arrhenius rate constants increase with increasing temperature, indicating positive activation energy. As a result, propene and related carboxylic acids are formed via a reaction path involving a six-membered ring. Experiments on real biofuels are difficult, both experimentally and computationally, due to the large molecules involved. As a result, model system studies are more efficient and effective in simulating the thermochemical and kinetic parameters of the considered compounds. The current study is the first to

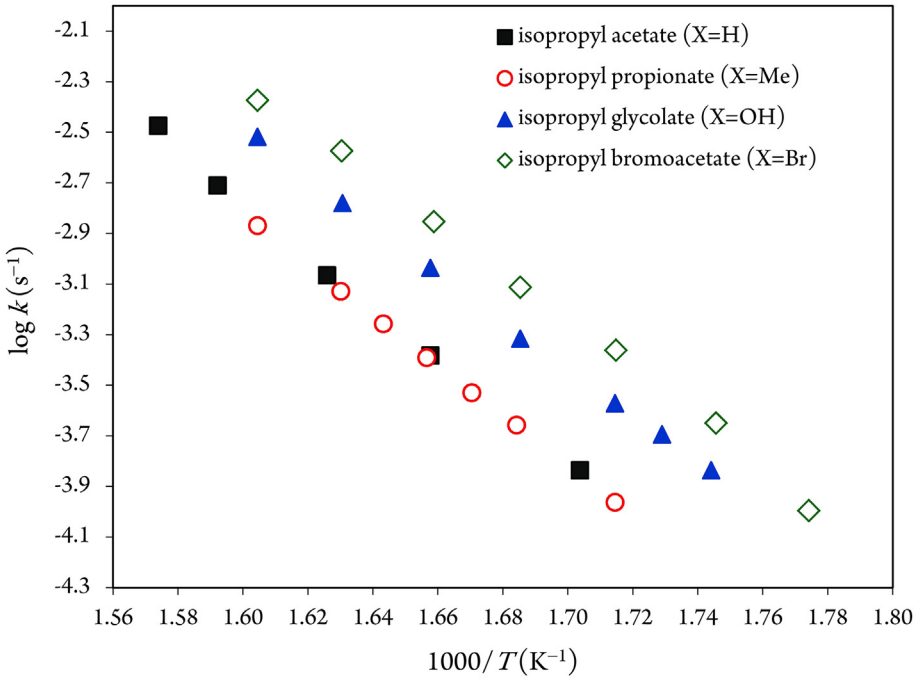

Figure 1. Arrhenius plot of the experimental rate constant for the pyrolysis of **IPA** and its derivatives [18].

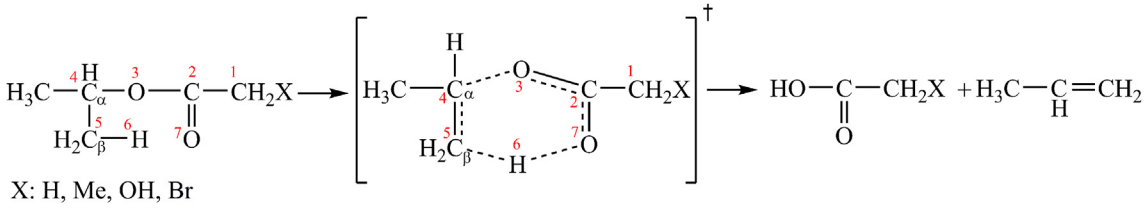

Scheme 2. Unimolecular decomposition processes of isopropyl acetate and its derivatives through the six-center reaction of the type (atom numbering of the studied compounds).

consider the unimolecular decomposition of **IPA** and its derivatives, which have the potential to be used as a biodiesel additive and model biodiesel [22]. The purpose of this research is to look into the activation energies, rate constants, and molecular mechanisms of the decomposition processes depicted in Scheme 2.

For this purpose, transition state theory (TST) [23, 24, 25, 26, 27, 28, 29, 30] will be used, along with the ωB97XD [31] and M06–2x functionals [32], and 6–311++G(d,p) diffuse function basis set [33, 34]. A comparison with more accurate energies from the CBS-QB3 method will be made for clarity of these reaction mechanisms and to determine which functional provides the most accurate reaction energies and energy barriers [35, 36]. Furthermore, to unravel the detailed available experimental data over the temperature range 563–623 K, rate constants are estimated using transition state theory (TST) at the high-pressure (HP) limit [23, 24, 25, 26, 27, 28], and their fall-off behavior is studied using RRKM theory at lower-pressures (LP) [37, 38, 39]. The M06–2x functional is frequently regarded as the best exchange-correlation functional for both thermodynamics and kinetics [32]. Finally, we will work to provide additional qualitative chemical insights into the involved reaction mechanisms by analyzing natural bond orbital (NBO) results [40, 41].

2. Theory and computational details

All molecular structures involved in pyrolysis processes were performed using DFT [42, 43] in combination with the ωB97XD and M06–2x functionals, with the split valence 6–311++G(d,p) basis set [44], due to its high accuracy in achieving geometries, zero-point vibrational energy (ZPVE) [45], and frequencies [46], combined with computational efficiency [47, 48]. The thermodynamic properties were determined using the vibrational analysis obtained previously for each stationary point. The presence of only one imaginary frequency was demonstrated in the case of the transition state structures. All molecules and radicals carried out in this study are considered neutral with charge zero while the multiplicities of the saturated molecules are 1 and 2 for radicals.

Because the studied DFT energies are insufficiently accurate, the electronic energies were further optimized using the CBS-QB3 composite method [49]. All quantum calculations were done with the Gaussian 09 package of programs [50], and all molecular structures were visualized with ChemCraft [51]. The CBS-QB3 method [52, 53, 54], is a benchmark approach for calibrating the accuracy of DFT methods. Harmonic vibrational frequencies were calculated to determine whether the identified stationary points were local minima or saddle points. Furthermore, the intrinsic reaction coordinate (IRC) calculation [55] was carried out with 61 points along the reaction path in both directions (forward and backward) to determine whether the discovered TS structure is connected to the reactant and corresponding products [56].

The temperatures used in the experiment [18] were used to calculate the unimolecular rate constants for the investigated reaction pathways. ZPVE contributions were considered when calculating activation energies. The rate constants for unimolecular reactions in the HP limit are defined by transition state theory as given in Eq. (1) [57, 58, 59].

$$k_{uni} = \kappa(T)\frac{\sigma k_B T}{h}\frac{Q^{\dagger}_{TS}}{Q_A}\exp(-E_a/RT) \quad (1)$$

where k_B and h denote Boltzmann's and Planck's constants, correspondingly. Here, $Q^{\dagger}_{TS}$ and Q_A represent the total partition function of the TS and the reactant, respectively, and σ denotes the reaction-path degeneracy. By integrating the probability of transmission, $p(E)$, which is identical to the over Boltzmann distribution of energies, the Eckart tunneling factor, $\kappa(T)$, is used to correct the calculated TST rate constants (Eq. (2)) [60]:

$$\kappa_{Eckart}(T) = \frac{\exp\left(\Delta H_f^{\neq,0K}/k_B T\right)}{k_B T}\int_o^{\infty} p(E)\exp(-E/k_B T)\,dE \quad (2)$$

where $\Delta H_f^{\neq,0K}$ denotes the zero-point corrected energy barriers in the forward direction computed by the KiSThelP package [61], to calculate rate coefficients at various temperatures [62, 63, 64, 65, 66, 67, 68, 69, 70]. In all calculations, a scaling factor of 0.99 was applied to the calculated frequencies using the CBS-QB3 method [71].

All rate constant values provided are the results of calculations performed using the TST and RRKM theory implementations. The energy-dependent microcanonical rate constants $k(E)$ are given by the standard RRKM expression (Eq. (3))

$$k(E) = \frac{\sigma N^{\dagger}(E)}{h\ \rho(E)} \quad (3)$$

where σ is the reaction pathway degeneracy, $N^{\dagger}(E)$ represents the total number of energy states of the TS, and $\rho(E)$ denotes the density of reactant states. Canonical rate constants $k(T)$ (Eq. (4)) are determined thereafter by state integration and Boltzmann averaging [72]:

$$k(T) = \frac{1}{Q(T)}\int_{E_o}^{\infty} k(E)\rho(E)\exp(-\beta E)\,dE \quad (4)$$

where $\beta = 1/k_B T$ and $Q(T)$ is the partition function of the reactants as obtained by Eq. (5) [73].

$$Q(T) = \int_o^{\infty} \rho(E)\exp(-\beta E)\,dE \quad (5)$$

The quantum mechanical tunneling contribution was modeled using an Eckart potential barrier height [74, 75]. With $\omega = \beta_c.Z_{LJ}$ [M] denoting the effective collision frequency, Z_{LJ} the Lennard-Jones collision frequency [M] the total gas concentration, and $\beta_c = 0.2$ the collisional efficiency, the strong collision approximation is used. Table 1 shows the

Table 1. Lennard-Jones potential parameters.

Species	LJ potential parameters	
	σ (Å)	ε/k_B (K)
isopropyl acetate (**1**)	5.6	436.8
isopropyl propionate (**2**)	5.9	454.4
isopropyl glycolate (**3**)	5.7	505.4
isopropyl bromoacetate (**4**)	5.9	504.5
Argon	3.465	113.5

collision frequencies (Z_{LJ}) calculated using the LJ parameters for argon (as a diluent gas) [76] and reactants [77].

3. Results and discussion

3.1. Energetic and thermodynamic parameters

Tables 3 and 4 summarize the activation and reaction parameters for the thermal decomposition of the studied compounds. According to the available experimental activation energies [18], decomposition of compounds **1**–**4** exhibits endothermic processes ($\Delta H > 0$) [with $\Delta H \approx$ 11.39–12.30, 11.80–11.83, 11.36–11.74, and 11.53–11.79 kcal mol^{-1} at the studied DFT methods, while ΔH is nearly equal to 11.73, 11.57, 11.54, and 10.70 kcal mol^{-1} when X = H, Me, OH, and Br, respectively at the CBS-QB3 method). Gibbs free reaction energies, ΔGs are positive (endoergic) for the decomposition of Isopropyl acetate (**1**) at all studied methods while ΔGs are negative for other pathways [**2**–**4**], hence these reactions are exergonic processes ($\Delta G < 0$) at a pressure of 1 bar and T = 298 K. According to the energy profiles in Table 2, the formation of $CH_3CH = CH_2$+$CH_2(Br)CO_2H$ species (**P4**) via pathway **4** appears to be more favorable in terms of kinetics and thermodynamic control than the other reactions at the CBS-QB3 method.

Activation parameters namely Gibbs free energy ($\Delta G^{\dagger}$) and enthalpy ($\Delta H^{\dagger}$) for reactions **1**–**4** are positive, indicating that activation processes require energy and are not spontaneous (see Table 3). It is expected that replacing the H atom with Me, OH, or Br will lower the energy barrier

Table 2. Reaction parameters (energy, enthalpy, and Gibbs free energy) (in kcal mol^{-1}) of compounds **1**–**4** at the studied DFT levels and the CBS-QB3 method (P = 1 bar).

Parameter Reaction	ωB97XD/6–311++G(d,p)			M06–2x/6–311++G(d,p)			CBS-QB3		
	ΔE_{0K}	ΔH°_{298K}	ΔG°_{298K}	ΔE_{0K}	ΔH°_{298K}	ΔG°_{298K}	ΔE_{0K}	ΔH°_{298K}	ΔG°_{298K}
Isopropyl acetate → **P1** [propene + Acetic acid]	11.488	11.385	0.282	11.926	12.299	0.162	11.440	11.734	0.277
Isopropyl propionate → **P2** [propene + Propionic acid]	11.475	11.829	−0.584	11.392	11.800	−1.572	11.366	11.571	−0.469
Isopropyl glycolate → **P3** [propene + Glycolic acid]	11.052	11.361	−0.919	11.374	11.744	−1.148	11.294	11.541	−0.841
Isopropyl bromoacetate → **P4** [propene + Bromoacetic acid]	11.370	11.529	−0.464	11.628	11.791	−0.257	10.596	10.698	−1.120

Table 3. Activation parameters (energy, enthalpy, and Gibbs free energy) (in kcal mol^{-1}), and activation entropy (in cal mol^{-1}K^{-1}) of compounds **1**–**4** at the studied DFT levels and the CBS-QB3 method (P = 1 bar).

Method Reaction	ωB97XD/6–311++G(d,p)				M06–2x/6–311++G(d,p)				CBS-QB3				Experiment ($\Delta E^{\dagger}$)
	$\Delta E_{0K}^{\dagger}$	$\Delta H_{298K}^{\dagger}$	$\Delta G_{298K}^{\dagger}$	$\Delta S_{298K}^{\dagger}$	$\Delta E_{0K}^{\dagger}$	$\Delta H_{298K}^{\dagger}$	$\Delta G_{298K}^{\dagger}$	$\Delta S_{298K}^{\dagger}$	$\Delta E_{0K}^{\dagger}$	$\Delta H_{298K}^{\dagger}$	$\Delta G_{298K}^{\dagger}$	$\Delta S_{298K}^{\dagger}$	
H–$CH_2CO_2CHMe_2$ → **TS1**	37.139	37.218	36.570	2.174	39.324	38.862	39.591	−2.446	40.268	40.291	39.703	1.971	(47.5 ± 1.9) [b]
Imaginary frequency TS1 (cm^{-1})	1317.86*i*				1426.77*i*				1261.81*i*				
CH_3–$CH_2CO_2CHMe_2$ → **TS2**	36.251	36.371	35.635	2.469	38.316	38.342	37.647	2.332	39.384	39.370	38.882	1.636	(45.4 ± 0.2)[a]
Imaginary frequency TS2 (cm^{-1})	1315.36*i*				1415.89*i*				1245.16*i*				
OH–$CH_2CO_2CHMe_2$ → **TS3**	35.203	35.254	34.675	1.942	37.578	37.577	37.129	1.506	38.579	38.564	38.074	1.648	(43.0 ± 0.7)[a]
Imaginary frequency TS3 (cm^{-1})	1256.18*i*				1382.79*i*				1230.76*i*				
Br–$CH_2CO_2CHMe_2$ → **TS4**	34.179	34.133	33.768	1.225	36.947	36.822	36.817	0.019	37.530	37.513	36.875	2.141	(43.3 ± 1.4)[a]
Imaginary frequency TS4 (cm^{-1})	1155.09*i*				1323.89*i*				1098.31*i*				

[a] Experimental values: Refs.: *a* [18], and *b* [19].

Table 4. Bond order analysis using NBO for reactions **1**–**4**.

Reaction	Bond	C_2–O_3	C_2–O_7	O_3–C_4	C_4–C_5	C_5–H_6	O_7–H_6	δB_{av}	S_y
Isopropyl acetate (**1**)	B_i(R)	1.0096	1.7789	0.8461	1.0192	0.9396	0.0000	0.491	0.90
	B_i(TS)	1.4208	1.3762	0.3013	1.3716	0.4822	0.2855		
	B_i(P)	1.7767	1.0274	0.0000	1.9884	0.0000	0.7518		
	%EV	53.60	53.59	64.39	36.36	48.68	37.98		
Isopropyl propionate (**2**)	B_i(R)	1.0107	1.7761	0.8458	1.0182	0.9386	0.0000	0.486	0.90
	B_i(TS)	1.4140	1.3771	0.3013	1.3680	0.4875	0.2812		
	B_i(P)	1.7761	1.0246	0.0000	1.9884	0.0000	0.7509		
	%EV	52.69	53.09	64.38	36.05	48.06	37.45		
Isopropyl glycolate (**3**)	B_i(R)	1.0035	1.8040	0.8453	1.0190	0.9411	0.0000	0.512	0.88
	B_i(TS)	1.4522	1.3620	0.2894	1.3722	0.4888	0.2784		
	B_i(P)	1.7535	1.0642	0.0000	1.9884	0.0000	0.7505		
	%EV	59.83	59.75	65.76	36.43	48.06	37.10		
Isopropyl bromoacetate (**4**)	B_i(R)	1.0136	1.7996	0.8373	1.0201	0.9385	0.0000	0.505	0.86
	B_i(TS)	1.4659	1.3677	0.2611	1.3724	0.5072	0.2593		
	B_i(P)	1.7724	1.0464	0.0000	1.9884	0.0000	0.7471		
	%EV	59.61	57.34	68.82	36.38	45.96	34.71		

while increasing the associated rate constants. The barrier energy ($\Delta E^{\dagger}_{0K}$) for the decomposition of compound **4** is lower by nearly 2.74, 1.85, and 1.05 kcal mol^{-1} at the CBS-QB3 method, respectively, than the energy barrier for the other species [**1**–**3**] which is consistent with the replacement of the H, Me, and OH groups by Br atom. Similar observations can be made when Gibbs free activation energies are considered: despite slightly lower entropies, the Gibbs free energy for the pyrolysis of isopropyl bromoacetate (nearly 33.76, 36.82, and 36.88 kcal mol^{-1} at the ωB97XD, M06–2x, and CBS-QB3, respectively) is lower than for isopropyl acetate (approximately 36.57, 39.59, and 39.70 kcal mol^{-1}, respectively at the same methods).

The kinetics of the decomposition is determined by the activation energy barrier and the activation entropy ($\Delta S^{\dagger}$) required to reach the TS structure [78, 79]. The activation entropies for the studied compounds [X–$CH_2COOCHMe_2$ with X = H (**1**), Me (**2**), OH (**3**), and Br (**4**)] are equal to 1.97, 1.64, 1.65, and 2.14 Cal $mol^{-1}K^{-1}$, respectively, at the CBS-QB3 method (see Table 3). Compound **4** has a higher activation entropy than compounds **1**–**3**, which could be a result of higher charge separation and thus a less restricted TS, or to larger restriction on rotations in this compound's initial state.

Compounds **1**–**4** have unimolecular decomposition processes that are concerted, six-center, and homolytic. The substitution of methyl, hydroxyl, and bromine groups for a hydrogen atom attached to a $–CH_2$ group is expected to lower the activation energy and thus increase the kinetic rate constant of the reaction. The influence of an ortho-bromine could be due to the halogen depolarizing the carbonyl group, which reduces the attraction of a hydrogen atom in β position to the carbonyl oxygen.

The OH and Br substituents tend to enhance the pyrolysis of the investigated esters in comparison to the parent isopropyl acetate, while the α-methyl group appears to decrease the kinetic rate constant. At room temperature, the sequence of kinetic rate constants as Br > OH > H > CH_3 has a direct relationship with acid strength [80]. Because electron withdrawal by the bromine substituent tends to enhance the ester's decomposition with respect to the parent compound isopropyl acetate, the kinetic rate constant for the decomposition of isopropyl bromoacetate (compound **4**) to the formation of propene and bromoacetic acid at T = 623.25 K is most favorable from a kinetic viewpoint, and the RRKM calculations show that low pressures around 0.01 bar are required to restore the validity of the TST approximation for this reaction channel.

Given that these secondary acetates' polar substituents appear to influence reaction rate constants, it is reasonable to believe that the polarization of the alkyl side's C–O bond length in the sense $–O{=}C–O^{-\delta}\ldots C^{+\delta}$ is the determining factor in the TS of the considered pathways [18].

3.2. Transition state and mechanism

The geometrical properties of the reactants (**R1**−**R4**), transition states (**TS1**−**TS4**), propene, and related acids (**P**) of the considered pathways are optimized using the CBS-QB3 method (see Scheme 2). The studied reactions lead to the cleavage of the O_3–C_4 and C_5–H_6 bonds through TS structures to produce propene and the related acid with reaction energy up to ~11.44 kcal mol^{-1} at the CBS-QB3 composite method. The transition state structure forms a six-membered ring. The O_3–C_4 bond length increases correspondingly up to ~0.71 Å, showing that this bond is broken in the TS structures. Similarly, the C_5–H_6 bond length increases by only ~0.2 Å. The O_3–C_4 and C_5–H_6 bond lengths are elongated by 2.157 and 1.293 Å in the transition states [**TS1**−**TS4**], respectively, while simultaneously shrinking the O_7–H_6 distance to form a new O_7–H_6 bond by 0.965 Å. Also, the bond lengths in the TS structures decrease from ~1.52 to ~1.41 Å that indicating a shift in the C_4–C_5 bond lengths from single to double bond characters. The bond distances of C_2–O_7 show that a shift from double bonds (1.271–1.273 Å) in the TS structures to single bonds (1.333–1.349 Å) in the related acid. The C_5–H_6 bond length is elongated by ~18% in such compounds to the calculated equilibrium structures for **R1**−**R4** molecules (1.093 Å). On the contrary, the O_7–H_6 bond forms quite naturally, and at a greater distance than in the reactants (see Figure 2).

Dihedral angles [φ (O_3–C_2–O_7–H_6)] for the chemical pathways **1–4** in TSs are 125.22° (112.77 to –12.45°), 129.67° (113.41 to −16.26°), 142.91° (126.65 to –16.26°), and 117.85° (105.38 to –12.47°), respectively at the CBS-QB3 method (see Table 3 and Figure 2 for atom numbering). These findings indicate that the TS structures for the decomposition reaction of compounds **1**–**4** are non-planar. The imaginary frequencies for the transition states of chemical channels **1**–**4** were also found to be 1262*i*, 1245*i*, 1231*i*, and 1098*i* cm^{-1}, respectively.

The n_T parameter (Eq. (6)) defines Hammond's postulate behavior along the reaction coordinate [81, 82].

$$n_T = \frac{1}{2 - (\Delta G_r / \Delta G^{\dagger})} \tag{6}$$

Eq. (6) states that the position of the TS structure along the reaction coordinate is solely determined by the ΔG_r and $\Delta G^{\dagger}$ as thermodynamic and kinetic quantities, respectively. When $n_T < 0.5$ (*early* TS), the TS structure is similar to reactant, while when $n_T > 0.5$, the TS structure is similar to product (*late* TS) [82]. In the thermal decomposition of compounds **1**–**4** **[**$R_i \rightarrow$ propene + P_i (i = 1–4)**]**, the TS structures are identical to the studied reactants and products, and the n_T values are around 0.5 using the CBS-QB3 method.

3.3. Bond order analysis

Bond order (B), a concept used to study the molecular mechanism of many reactions, provides a more balanced measure of the extent of bond formation/breaking along the reaction [83]. Wiberg bond indices [84] were calculated using an NBO analysis [85]. Several bond-forming/breaking processes occur during fragmentation, and the overall nature of the pyrolysis reaction can be monitored using the synchronicity (S_y) index as given in Eq. (7) [86].

$$S_y = 1 - \frac{\left[\sum_{i=1}^{n} \frac{|\delta B_i - \delta B_{av}|}{\delta B_{av}}\right]}{2n - 2} \tag{7}$$

where n is the number of direct bonds in the chemical process, δB_i denotes the bond index's relative variation at the TS for a bond i, and δB_{av} represents the average change in bond orders. It is noted that the synchronicity parameter, S_y ranges from 0 (fully asynchronous process) to 1 (fully concerted synchronic process) [87].

Bond indices were calculated for the bonds involved in the studied reactions, *i.e.* C_2–O_3, C_2–O_7, O_3–C_4, C_4–C_5, C_5–H_6, and O_7–H_6 (see Scheme 2). All other bonds are essentially unchanged. The calculated Wiberg bond indices, B_i allow us to examine the progress of the reaction and assess the position of the TSs between reactants and products (Table 4). The pyrolysis of the **IPA** and its derivatives [X–$CH_2CO_2CHMe_2$ with X = Me, OH, and Br] implies the cleavage of the O_3–C_4 and C_5–H_6 bonds yielding products located at 11.44, 11.37, 11.29, and 10.60 kcal mol^{-1} above the reactants, respectively, at the CBS-QB3 method. The formation of the C=C double bond results in the elongation of the bond breaking of C_5–H_6 and O_3–C_4, as well as the simultaneous shortening of the bond lengths of C_4–C_5 (Table 4).

The most advanced reaction coordinate for pyrolysis of compounds **1**–**4**, according to Wiberg bond indices, O_3–C_4 bond breaking (%EV = 64.38–68.82). The progress in C_5–H_6 bond breaking is also significant (%EV = 45.96–48.68). For the investigated reactions, there is less progress in the formation of C_4–C_5 double bonds (%EV = 36.05–36.38). The synchronicity indices for reactions **1**–**4** are 0.90, 0.90, 0.88, and 0.86, indicating that the studied reactions are concerted and slightly asynchronous, respectively.

The distribution of electrons during the decomposition reactions of **IPA** and its derivatives can also be studied using charges. In this

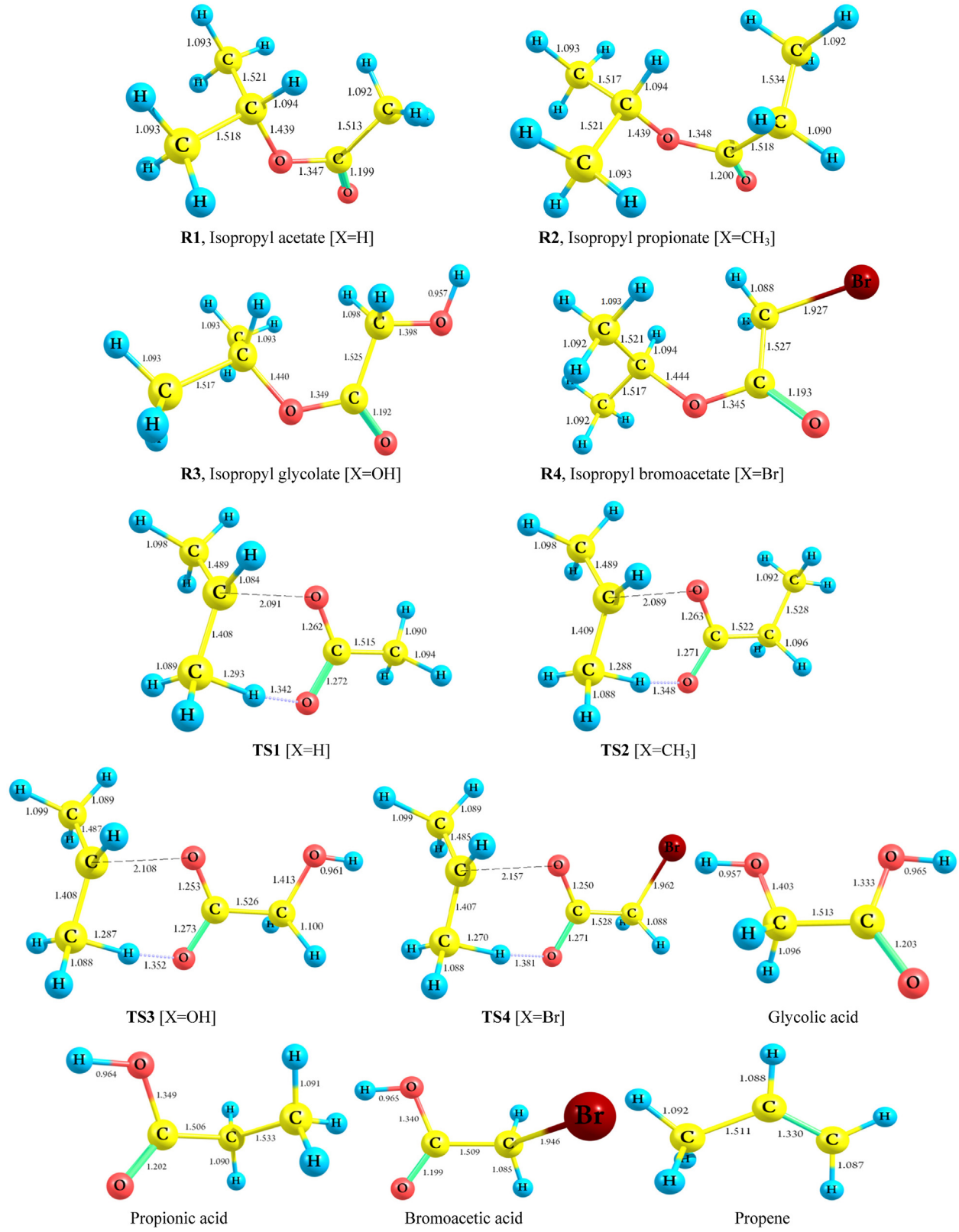

Figure 2. Stationary points that are involved in reactions **1**–**4** using the CBS-QB3 method [Bond lengths are given in angstroms (Å) and bond angles in degrees (°)].

regard, NBO charges have proven useful [78]. In all reactants, the O_3–C_4 bond is polarized (O_3 charge is −0.5783 to −0.5702 and C_4 is 0.1468–0.1485, charge separation Δq = 0.7187–0.7251) in the sense $O_3^{\delta-}$–$C_4^{\delta+}$. The following partial charges occur as the considered reaction progresses from reactants to transition states: an increase in negative charge δ^- in oxygen O_3 [(−0.5783 to −0.5702) in reactants compared to (–0.6573 to –0.6305) in TSs] as O_3–C_4 bond breaks, an increase in positive charges δ^+ in carbon C_4 [(0.1468–0.1485) in the reactants associated with (0.1793–0.1983) in TS] are summarized in Table 5.

Table 5. NBO charges of reactants (**R**) and transition states (**TS**) for the pyrolysis of reactions **1**–**4** at the CBS-QB3 method.

atom	1 (X = H)		2 (X = Me)		3 (X = OH)		4 (X = Br)	
	R1	TS1	R2	TS2	R3	TS3	R4	TS4
C_1	0.8294	−0.6711	−0.4899	−0.4740	−0.1331	−0.1112	−0.5415	−0.4994
C_2	0.8294	0.8446	0.8324	0.8492	0.8077	0.8214	0.8092	0.8174
O_3	−0.5759	−0.6521	−0.5758	−0.6573	−0.5783	−0.6305	−0.5702	−0.6401
C_4	0.1485	0.1793	0.1482	0.1828	0.1468	0.1850	0.1474	0.1983
C_5	−0.5824	−0.7264	−0.5813	−0.7260	−0.5820	−0.7239	−0.5824	−0.7180
H_6	0.2033	0.3964	0.2056	0.3951	0.2043	0.3962	0.2072	0.3930
O_7	−0.5682	−0.6894	−0.5742	−0.6911	−0.5402	−0.6990	−0.5434	−0.6869

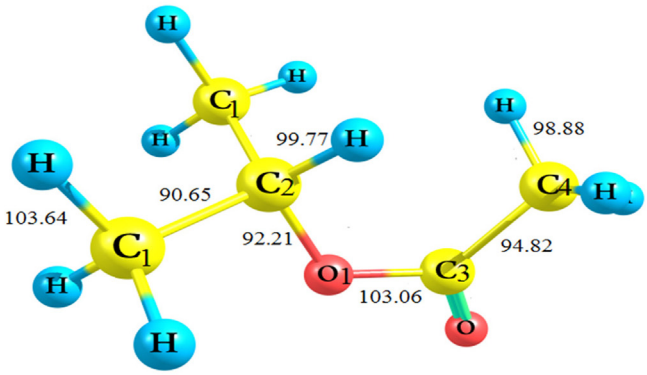

Compound 1, Isopropyl acetate [X=H]

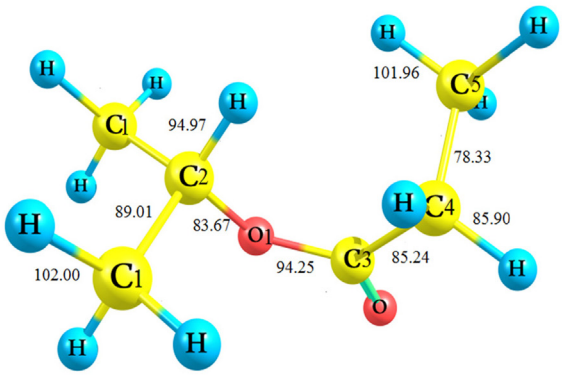

Compound 2, Isopropyl propionate [X=CH_3]

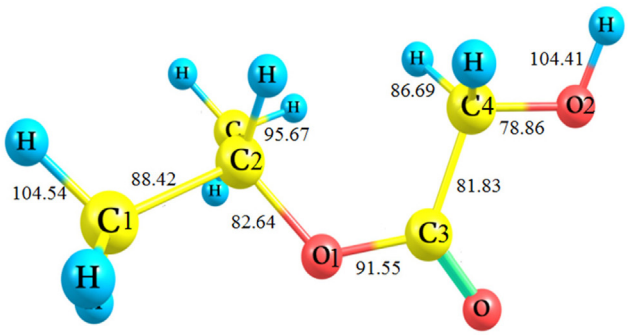

Compound 3, Isopropyl glycolate [X=OH]

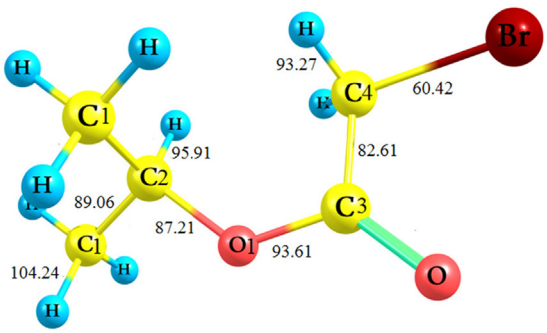

Compound 4, Isopropyl bromoacetate [X=Br]

Figure 3. BDEs (in kcal mol^{-1}) of the studied compounds at the CBS-QB3 method.

The C_α−O bond elongation [C_4–O_3] and successive polarization in the $C_\alpha^{+\delta}\ldots O^{-\delta}$ denotes the rate-determining step in the studied reactions (Scheme 2). Polarization of the $C_\alpha^{+\delta}\ldots O^{-\delta}$ bond can result from electron transmission toward the more electronegative group, and to a lesser extent, larger π-electron delocalization of the C=O group. As a result, the partially negatively charged oxygen atom of acetate (O_3) would face greater difficulty in stabilizing its *p* electrons toward the C=O group's adjacent more π-bonded carbon [5]. Thus, the more electronegative the substituent, the less stable the oxygen *p* electrons of the C_α−O bond toward the carbonyl carbon and the slower the rate constant [88].

3.4. Bonds dissociation energies (BDEs)

Estimating BDEs can provide early insights into bond strength and fuel behavior at high ignition temperatures [89, 90, 91, 92, 93]. The CBS-QB3 energies were used to calculate the BDEs of the considered compounds at $T = 298$ K as depicted in Figure 3.

The C_4−X bond is the weakest bond compounds **2**, **3,** and **4**, with 78.3, 78.9, and 60.4 kcal mol^{-1}, correspondingly, followed by comparable C_3–C_4 bond breaking with 81.8 and 82.6 kcal mol^{-1} for compounds **3** and **4**, individually, while in compound **1**, C_1–C_2 bond is the weakest bond with 90.7 kcal mol^{-1}, followed by C_2–O_1 bond energy 92.2 kcal mol^{-1}. For all investigated molecules, the internal C_4–H bond is the most accessible for H-atom removal with different oxidizing agents, while the terminal C_1–H bond is the most difficult.

3.5. Kinetic parameters

The CBS-QB3 method was used to calculate the TST and RRKM rate coefficients for the pyrolysis reactions of compounds **1**–**4** at $P = 1$ bar and the available experimental temperatures [18] (see Table 6 and Tables S1*a*–*d* of the Supplementary material contains additional RRKM data for the same temperatures computed at lower and higher pressures). The rate coefficient for the production of bromoacetic acid and propene

Table 6. Unimolecular rate constants (in s^{-1}) for the studied reactions using TST and RRKM (P = 1 bar).

Path T (°C)	TST				RRKM			
	R1 → P1	R2 → P2	R3 → P3	R4 → P4	R1 → P1	R2 → P2	R3 → P3	R4 → P4
290 (563 K)	5.39×10^{-1}	1.17×10^{0}	1.91×10^{0}	1.24×10^{1}	3.66×10^{-1}	7.95×10^{-1}	1.32×10^{0}	4.57×10^{0}
295 (568 K)	7.16×10^{-1}	1.54×10^{0}	2.51×10^{0}	1.61×10^{1}	4.90×10^{-1}	1.06×10^{0}	1.74×10^{0}	5.99×10^{0}
300 (573 K)	9.48×10^{-1}	2.02×10^{0}	3.28×10^{0}	2.09×10^{1}	6.52×10^{-1}	1.39×10^{0}	2.29×10^{0}	7.81×10^{0}
305 (578 K)	1.25×10^{0}	2.64×10^{0}	4.27×10^{0}	2.70×10^{1}	8.64×10^{-1}	1.83×10^{0}	3.00×10^{0}	1.01×10^{1}
310 (583 K)	1.64×10^{0}	3.43×10^{0}	5.53×10^{0}	3.47×10^{1}	1.14×10^{0}	2.40×10^{0}	3.91×10^{0}	1.31×10^{1}
315 (588 K)	2.13×10^{0}	4.44×10^{0}	7.13×10^{0}	4.45×10^{1}	1.50×10^{0}	3.13×10^{0}	5.07×10^{0}	1.68×10^{1}
320 (593 K)	2.77×10^{0}	5.73×10^{0}	9.16×10^{0}	5.67×10^{1}	1.95×10^{0}	4.05×10^{0}	6.55×10^{0}	2.16×10^{1}
325 (598 K)	3.58×10^{0}	7.35×10^{0}	1.17×10^{1}	7.20×10^{1}	2.54×10^{0}	5.24×10^{0}	8.42×10^{0}	2.75×10^{1}
330 (603 K)	4.62×10^{0}	9.41×10^{0}	1.49×10^{1}	9.12×10^{1}	3.29×10^{0}	6.74×10^{0}	1.08×10^{1}	3.50×10^{1}
335 (608 K)	5.92×10^{0}	1.20×10^{1}	1.89×10^{1}	1.15×10^{2}	4.25×10^{0}	8.63×10^{0}	1.38×10^{1}	4.43×10^{1}
340 (613 K)	7.57×10^{0}	1.52×10^{1}	2.39×10^{1}	1.44×10^{2}	5.46×10^{0}	1.10×10^{1}	1.75×10^{1}	5.59×10^{1}
345 (618 K)	9.64×10^{0}	1.92×10^{1}	3.01×10^{1}	1.81×10^{2}	6.98×10^{0}	1.40×10^{1}	2.21×10^{1}	7.02×10^{1}
350 (623 K)	1.22×10^{1}	2.42×10^{1}	3.78×10^{1}	2.25×10^{2}	8.90×10^{0}	1.77×10^{1}	2.79×10^{1}	8.79×10^{1}

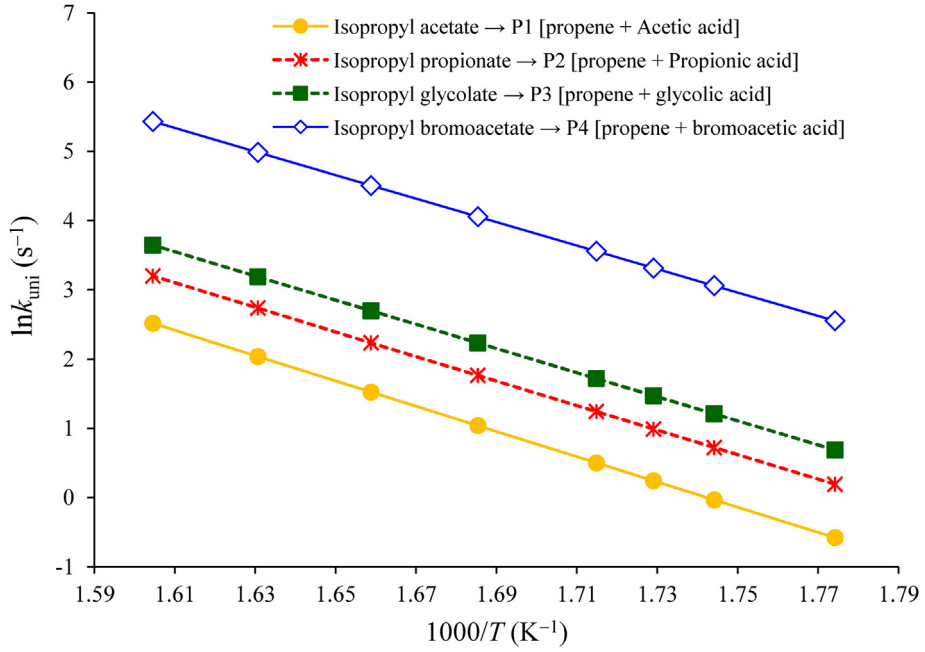

Figure 4. Arrhenius plot of the measured TST rate constants [for R_i (i = 1–4) →propene + related acid] (P = 1 bar).

species [via **R4**] is larger than that obtained for the acetic acid, propionic acid, and glycolic acid species [via **R1**−**R3**, respectively], which corresponds to a decrease in energy barrier of 2.74, 1.85, and 1.05 kcal mol^{-1} on the related reactions. Indeed, the TST results reveal that reaction **4** has higher rate constants than the other pathways. These rate constants gradually increase with increasing temperature due to the positive energy barriers involved. Furthermore, the entropy loss of the studied cyclic TSs at the CBS-QB3 method is low, as expected.

According to Table 6, TST overestimates the RRKM rate constants by 2.78 orders of magnitude, indicating that RRKM theory should be used to investigate the fall-off behavior of these rate constants towards the low-pressure limit. Based on the computed CBS-QB3 energy profiles, all calculated temperature-dependent TST rate constants for the considered reactions, confirm that the production of propene and bromoacetic acid species (via **R4**) is the fastest under atmospheric pressure at all studied temperatures (see Figure 4). The same holds for pressures ranging from 10^{-10}–10^{2} bars (see Tables S1*a*−*d* in the Supplementary material). Because the energy barriers involved are high, the rate constants for the formation of the "acetic acid", "propionic acid" and "glycolic acid" species are lower at the studied temperatures than the rates for the formation of the "bromoacetic acid" species: the rates describing the pyrolysis of isopropyl bromoacetate into propene + bromoacetic acid species are up to two orders of magnitude lower (reaction **4**). As shown in Figure 4 and Table 6, the temperature dependence of the RRKM rate constants for reactions **1**–**4** over temperature ranges 563–623 K was investigated with an interval of 5 K, revealing that rate constants increase with increasing temperature.

The RRKM equation modeling revealed that at atmospheric and higher/lower troposphere pressures, the rate constants of reaction are in the fall-off regime. Figure 5 shows additional fall-off curve plots for the RRKM rate constants (k_{uni}). Pressures greater than 0.01 bar appear to be required for ensuring saturation to the high-pressure limit of the RRKM rate constants, by rather larger energy barriers ranging from 37.53 to 40.27 kcal mol^{-1}. However, when compared to RRKM data, the TST approximation breaks down at pressures less than 0.01 bar for the kinetic rate coefficient of reaction **4**.

Table 6 shows that kinetic rates calculated at a pressure of 1 bar using the TST and RRKM approaches with the same energy profiles do not vary significantly. It is thus better to use the RRKM approach to evaluate rate constants because the strong pressure dependence of rate constants can

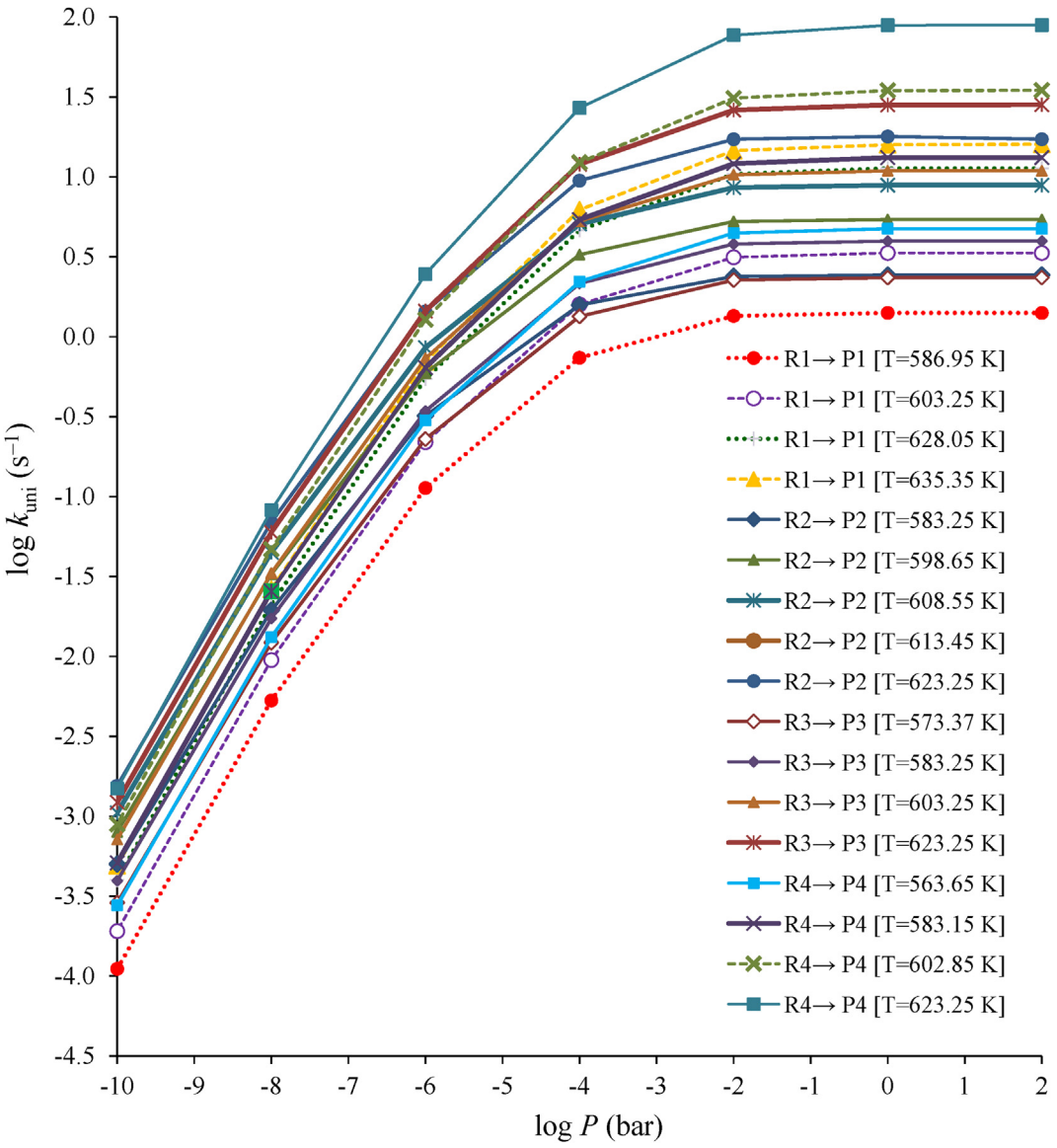

Figure 5. Fall-off plots for the rate constants as a function of pressure for the thermal decomposition processes of compounds **1**–**4** using RRKM theory calculated at the CBS-QB3 method.

be accounted for at pressures less than 0.01 bar. The effect of Eckart tunneling appears to be (almost) negligible and has only a minor impact on the computed rate constants (see Table S2 of the Supplementary material). Based on the computed CBS-QB3 energy profiles and B3LYP/6–311++G(d,p) vibrational frequencies, TST calculations of the rates that characterize the studied reaction pathways yielded $\kappa(T)$ values ranging from 1.3 to 1.5. As the temperature increases from 563 to 623 K, the ratios of TST and RRKM estimates of rate constants for reaction 4 decrease from 2.71 to 2.56. These variations are caused by tunneling corrections to the TST rate constants.

4. Conclusions

The thermal decomposition of isopropyl acetate and its derivatives [X: Me, OH, and Br] in the gas phase was investigated at the ωB97XD/6–311++G** and M06–2x/6–311++G** levels of theory as well as CBS-QB3 composite method. At the high-pressure limit, unimolecular rate coefficients were calculated using transition state theory (TST). RRKM theory was used to investigate their pressure dependence in the pressure range 10^{-10}–10^{2} bar and at available experimental temperatures. According to the data provided, the reaction [isopropyl bromoacetate → propene + bromoacetic acid] is more favorable than the other reactions in terms of both thermodynamics and kinetics. The calculated energy barriers and unimolecular rates agree reasonably well with the experiment. These reactions' transition states correspond to non-planar six-membered cyclic structures. The use of synchronicity indices to analyze the computed pathways reveals concerted and slightly asynchronous processes. TST and RRKM theories were used to calculate rate constants under atmospheric pressure and in the fall-off regime, respectively, to supplement the calculated energy profiles. According to the RRKM calculations, pressures greater than 0.01 bar are sufficient to ensure the validity of the TST approximation for all studied reactions.

The most significant difference is seen in the O_3–C_4 bond length, which is elongated in the TSs (at 2.039–2.993 Å) when compared with the reactant distances (1.437–1.442 Å). When compared to other reaction changes, the TS structures show more progress in breaking the O_3–C_4 bond. According to the NBO charges analysis, the polarization of this bond in the sense $O_3^{\delta-}$–$C_4^{\delta+}$ is the determining factor in the pyrolysis process. A six-membered cyclic transition state is used to determine the rate of these reactions. The analysis of NBO charges shows that as the

O_3–C_4 bond breaks, carbon C_4 becomes more positively charged, and oxygen atom O_3 becomes more negatively charged in TSs.

Declarations

Author contribution statement

S.H. Reza Shojaei, Abolfazl Shiroudi, Mohamed A. Abdel-Rahman: Conceived and designed the experiments; Performed the experiments; Analyzed and interpreted the data; Contributed reagents, materials, analysis tools or data; Wrote the paper.

Funding statement

This research did not receive any specific grant from funding agencies in the public, commercial, or not-for-profit sectors.

Data availability statement

Data included in article/supplementary material/referenced in article.

Declaration of interests statement

The authors declare no conflict of interest.

Additional information

Supplementary content related to this article has been published online at https://doi.org/10.1016/j.heliyon.2022.e11274.

Acknowledgements

The authors dedicate this manuscript to the soul of Prof. Dr. Ahmed El-Nahas, the father of computational chemistry in Egypt, who recently died in an accident. May his soul rest in peace.

References

[1] R.B. Anderson, H.H. Rowley, Kinetics of the thermal decomposition of *n*-propyl and isopropyl formats, J. Phys. Chem. A 47 (1943) 454–463.
[2] E.M. Bilger, H. Hibbert, Mechanism of organic reactions. IV. Pyrolysis of esters and acetals, J. Am. Chem. Soc. 58 (1936) 823–826.
[3] C.D. Hurd, F.H. Blunk, The pyrolysis of esters, J. Am. Chem. Soc. 60 (1938) 2419–2425.
[4] R.F. Makens, W.G. Eversole, Kinetics of the thermal decomposition of ethyl formate, J. Am. Chem. Soc. 61 (1939) 3203–3206.
[5] G.G. Smith, W.H. Wetzel, The effect of molecular size and structure on the pyrolysis of esters, J. Am. Chem. Soc. 79 (1959) 875–879.
[6] B.A. Kumgeh, J.M. Bergthorson, Structure-reactivity trends of C1–C4 alkanoic acid methyl esters, Combust. Flame 158 (2011) 1037–1048.
[7] B. Yang, C.K. Westbrook, T.A. Cool, N. Hansen, H.K. Kohse, The effect of carbon-carbon double bonds on the combustion chemistry of small fatty acid esters, Z. Phys. Chem. 225 (2011) 1293–1314.
[8] T. Tan, X. Yang, Y. Ju, E.A. Carter, Ab initio pressure-dependent reaction kinetics of methyl propanoate radicals, Phys. Chem. Chem. Phys. 17 (2015) 31061–31072.
[9] W.K. Metcalfe, S. Dooley, H.J. Curran, J.M. Simmie, A.M. El-Nahas, M.V. Navarro, Experimental and modeling study of $C_5H_{10}O_2$ ethyl and methyl esters, J. Phys. Chem. A 111 (2007) 4001–4014.
[10] A.M. Silva, A theoretical study of the pyrolysis of isopropyl acetate, Chem. Phys. Lett. 439 (2007) 8–13.
[11] M.A.G. de Sarmiento, R.M. Domınguez, G. Chuchani, Electronic effects of polar substituents at the acyl carbon. The pyrolysis kinetics of several isopropyl esters, J. Phys. Chem. A 84 (1980) 2531–2535.
[12] R. Taylor, The mechanism of the gas-phase pyrolysis of esters. Part 7. The effects of substituents at the acyl carbon, J. Chem. Soc. Perkin Trans 2 (1978) 1255–1258.
[13] J.C. Scheer, E.C. Kooyman, F.L. Sixma, Gas phase pyrolysis of alkyl acetates, Recl. TraV. Chim. Pays-Bas. 82 (1963) 1123–1154.
[14] E.U. Emovon, A. Maccoll, Gas-phase eliminations. Part III. The pyrolysis of some secondary and tertiary alkyl acetates, J. Chem. Soc. (1962) 335–340.
[15] H.Y. Lee, I.K. Lai, H.P. Huang, I.L. Chien, Design and control of thermally coupled reactive distillation for the production of isopropyl acetate, Ind. Eng. Chem. Res. 51 (2012) 11753–11763.
[16] B.J. Zhang, W.S. Yang, S. Hu, Y.Z. Liang, Q.L. Chen, A reactive distillation process with a side draw stream to enhance the production of isopropyl acetate, Chem. Eng. Process 70 (2013) 117–130.
[17] M.A. Abdel-Rahman, A. Shiroudi, S. Kaya, A.M. El-Nahas, Theoretical investigations on the unimolecular decomposition mechanisms of isopropyl acetate, J. Mol. Struct. 1262 (2022), 133006.
[18] G. Chuchani, I. Martin, M. Yepez, M.J. Diaz, Kinetics of the gas-phase pyrolysis of some secondary acetates, React. Kinet. Catal. Lett. 6 (1977) 449–454.
[19] A.T. Blades, The kinetics of the pyrolysis of ethyl and isopropyl formates and acetates, Can. J. Chem. 32 (1954) 366–372.
[20] E.U. Emovon, Pyrolyses of some *t*-butyl derivatives, J. Chem. Soc. (1963) 1246–1250.
[21] A. Maccoll, Gas-phase eliminations. Part I. The unimolecular gas-phase pyrolysis of some esters and analogous compounds, J. Chem. Soc. (1958) 3398–3402.
[22] A. Shiroudi, K. Hirao, K. Yoshizawa, M. Altarawneh, M.A. Abdel-Rahman, A.B. El-Meligy, A.M. El-Nahas, A computational study on the kinetics of pyrolysis of isopropyl propionate as a biodiesel model: DFT and ab initio investigation, Fuel 281 (2022), 118798.
[23] H. Eyring, The activated complex in chemical reactions, J. Chem. Phys. 3 (1935) 107–115.
[24] H.S. Johnston, Gas Phase Reaction Rate Theory, Roland Press, New York, 1966.
[25] K.J. Laidler, Theories of Chemical Reaction Rates, McGraw-Hill, New York, 1969.
[26] R.E. Weston, H.A. Schwartz, Chemical Kinetics, Prentice-Hall, New York, 1972.
[27] D. Rapp, Statistical Mechanics, Holt Rinehart & Winston, New York, 1972.
[28] E.E. Nikitin, Theory of Elementary Atomic and Molecular Processes in Gases, Clarendon Press, Oxford, 1974.
[29] I.W.M. Smith, Kinetics and Dynamics of Elementary Gas Reactions, Butterworths, London, 1980.
[30] A.E. Reed, L.A. Curtiss, F. Weinhold, Intermolecular interactions from a natural bond orbital, donor-acceptor viewpoint, Chem. Rev. 88 (1988) 899–926.
[31] J.D. Chai, M. Head-Gordon, Long-range corrected hybrid density functionals with damped atom-atom dispersion corrections, Phys. Chem. Chem. Phys. 10 (2008) 6615–6620.
[32] Y. Zhao, D.G. Truhlar, The M06 suite of density functionals for main group thermochemistry, thermochemical kinetics, noncovalent interactions, excited states, and transition elements: two new functionals and systematic testing of four M06-class functionals and 12 other functionals, Theor. Chem. Acc. 120 (2008) 215–241.
[33] M.J. Frisch, J.A. Pople, J.S. Binkley, Self-consistent molecular orbital methods 25. Supplementary functions for Gaussian basis sets, J. Chem. Phys. 80 (1984) 3265–3269.
[34] EMSL Basis Set Library. Basis Set Exchange. https://www.basissetexchange.org.
[35] J.A. Montgomery, M.J. Frisch, J.W. Ochterski, G.A. Petersson, A complete basis set model chemistry. VI. Use of density functional geometries and frequencies, J. Chem. Phys. 110 (1999) 2822–2827.
[36] J.A. Montgomery, M.J. Frisch, J.W. Ochterski, G.A. Petersson, A complete basis set model chemistry. VII. Use of the minimum population localization method, J. Chem. Phys. 112 (2000) 6532–6542.
[37] P.J. Robinson, K.A. Holbrook, Unimolecular Reactions, Wiley, New York, 1972.
[38] J.I. Steinfeld, J.S. Francisco, W.L. Hase, Chemical Kinetics and Dynamics, Prentice-Hall, Englewood Cliffs, New Jersey, 1999.
[39] H. Eyring, S.H. Lin, S.M. Lin, Basic Chemical Kinetics, Wiley, New York, 1980.
[40] A.E. Reed, R.B. Weinstock, F. Weinhold, Natural population analysis, J. Chem. Phys. 83 (1985) 735–746.
[41] J.K. Badenhoop, F. Weinhold, Natural steric analysis of internal rotation barriers, Int. J. Quant. Chem. 72 (1999) 269–280.
[42] S. Knippenberg, M.V. Bohnwagner, P.H. Harbach, A. Dreuw, Strong electronic coupling dominates the absorption and fluorescence spectra of covalently bound BisBODIPYs, J. Phys. Chem. A 119 (2015) 1323–1331.
[43] M. Frenette, M. Hatamimoslehabadi, S. Bellinger-Buckley, S. Laoui, J. La, S. Bag, S. Mallidi, T. Hasan, B. Bouma, C. Yelleswarapu, J. Rochford, Shining light on the dark side of imaging: excited state absorption enhancement of a bis-styryl BODIPY photoacoustic contrast agent, J. Am. Chem. Soc. 136 (2014) 15853–15856.
[44] T.H. Dunning, Gaussian basis sets for use in correlated molecular calculations. I. The atoms boron through neon and hydrogen, J. Chem. Phys. 90 (1989) 1007–1023.
[45] A.G. Baboul, L.A. Curtiss, P.C. Redfern, K. Raghavachari, Gaussian-3 theory using density functional geometries and zero-point energies, J. Chem. Phys. 110 (1999) 7650–7657.
[46] M. Halls, J. Velkovski, H. Schlegel, Harmonic frequency scaling factors for Hartree-Fock, S-VWN, B-LYP, B3-LYP, B3-PW91 and MP2 with the Sadlej pVTZ electric property basis set, Theor. Chem. Acc. 105 (2001) 413–421.
[47] J.P. Senosiain, S.J. Klippenstein, J.A. Miller, The reaction of acetylene with hydroxyl radicals, J. Phys. Chem. A 109 (2005) 6045–6055.
[48] E.E. Greenwald, S.W. North, Y. Georgievskii, S.J. Klippenstein, A two transition state model for radical-molecule reactions: a case study of the addition of OH to C_2H_4, J. Phys. Chem. A 109 (2005) 6031–6044.
[49] S. Pan, L. Wang, Atmospheric oxidation mechanism of *m*-xylene initiated by OH radical, J. Phys. Chem. A 118 (2014) 10778–10787.
[50] M.J. Frisch, G.W. Trucks, H.B. Schlegel, G.E. Scuseria, M.A. Robb, J.R. Cheeseman, G. Scalmani, V. Barone, B. Mennucci, G.A. Petersson, H. Nakatsuji, M. Caricato, X. Li, H.P. Hratchian, A.F. Izmaylov, J. Bloino, G. Zheng, J.L. Sonnenberg, M. Hada, M. Ehara, K. Toyota, R. Fukuda, J. Hasegawa, M. Ishida, T. Nakajima, Y. Honda, O. Kitao, H. Nakai, T. Vreven, J.A. Montgomery, J.E. Peralta, F. Ogliaro, M. Bearpark, J.J. Heyd, E. Brothers, K.N. Kudin, V.N. Staroverov, R. Kobayashi, J. Normand, K. Raghavachari, A. Rendell, J.C. Burant, S.S. Iyengar, J. Tomasi, M. Cossi, N. Rega, J.M. Millam, M. Klene, J.E. Knox, J.B. Cross, V. Bakken,

C. Adamo, J. Jaramillo, R. Gomperts, R.E. Stratmann, O. Yazyev, A.J. Austin, R. Cammi, C. Pomelli, J.W. Ochterski, R.L. Martin, K. Morokuma, V.G. Zakrzewski, G.A. Voth, P. Salvador, J.J. Dannenberg, S. Dapprich, A.D. Daniels, O. Farkas, J.B. Foresman, J.V. Ortiz, J. Cioslowski, D.J. Fox, Gaussian 09, Revision A.1, Gaussian Inc., Wallingford, 2009.

[51] G.A. Zhurko, Chemcraft Program v.1.6, 2014. https://www.chemcraftprog.com.

[52] A. Shiroudi, M.S. Deleuze, Theoretical study of the oxidation mechanisms of thiophene initiated by hydroxyl radicals, J. Mol. Model. 21 (2015) 301.

[53] M.R. Nyden, G.A. Petersson, Complete basis set correlation energies. I. The asymptotic convergence of pair natural orbital expansions, J. Chem. Phys. 75 (1981) 1843–1862.

[54] G.A. Petersson, M.A. Al-Laham, A complete basis set model chemistry. II. open-shell systems and the total energies of the first-row atoms, J. Chem. Phys. 94 (1991) 6081–6090.

[55] (a) C. Gonzalez, H.B. Schlegel, An improved algorithm for reaction path following, J. Chem. Phys. 90 (1989) 2154–2161;
(b) C. Gonzalez, H.B. Schlegel, Reaction path following in mass-weighted internal coordinates, J. Phys. Chem. A 94 (1990) 5523–5527.

[56] (a) H.P. Hratchian, H.B. Schlegel, Theory and Applications of Computational Chemistry: the First 40 Years, Elsevier, Amsterdam, 2005;
(b) H.P. Hratchian, H.B. Schlegel, Using Hessian updating to increase the efficiency of a Hessian based predictor-corrector reaction path following method, J. Chem. Theor. Comput. 1 (2005) 61–69.

[57] R. Chang, Physical Chemistry for the Biosciences, University Science Books, Sausalito, California, 2005.

[58] J.W. Moore, R.G. Pearson, Kinetics and Mechanism-The Study of Homogeneous Chemical Reactions, Wiley, New York, 1981.

[59] H.H. Carstensen, A.M. Dean, O. Deutschmann, Rate constants for the H abstraction from alkanes (R–H) by R′O2 radicals: a systematic study on the impact of R and R′, Proc. Combust. Inst. 31 (2007) 149–157.

[60] C. Eckart, The penetration of a potential barrier by electrons, Phys. Rev. 35 (1930) 1303–1309.

[61] S. Canneaux, F. Bohr, E. Henon, KiSThelP: a program to predict thermodynamic properties and rate constants from quantum chemistry results, J. Comput. Chem. 35 (2014) 82–93.

[62] A. Shiroudi, M.S. Deleuze, Theoretical study of the oxidation mechanisms of naphthalene initiated by hydroxyl radicals: the H-abstraction pathway, J. Phys. Chem. A 118 (2014) 3625–3636.

[63] A. Shiroudi, M.S. Deleuze, S. Canneaux, Theoretical study of the oxidation mechanisms of naphthalene initiated by hydroxyl radicals: the OH-addition pathway, J. Phys. Chem. A 118 (2014) 4593–4610.

[64] A. Shiroudi, M.S. Deleuze, S. Canneaux, Theoretical study of the oxidation mechanisms of naphthalene initiated by hydroxyl radicals: the O_2 addition reaction pathways, Phys. Chem. Chem. Phys. 17 (2015) 13719–13732.

[65] A. Shiroudi, M.S. Deleuze, Reaction mechanisms and kinetics of the isomerization processes of naphthalene peroxy radicals, Comput. Theor. Chem. 1074 (2015) 26–35.

[66] A. Shiroudi, E. Zahedi, A.R. Oliaey, M.S. Deleuze, Reaction mechanisms and kinetics of the elimination processes of 2-chloroethylsilane and derivatives: a DFT study using CTST, RRKM, and BET theories, Chem. Phys. (2017) 485–486, 140–148.

[67] A.R. Oliaey, A. Shiroudi, E. Zahedi, M.S. Deleuze, Theoretical study on the mechanisms and kinetics of the β-elimination of 2,2-dihaloethyltrihalosilanes (X= F, Cl, Br) compounds: a DFT study along with a natural bond orbital analysis, React. Kinet. Mech. Catal. 124 (2018) 27–44.

[68] M. Nayebzadeh, M. Vahedpour, A. Shiroudi, J.M. Rius-Bartra, Kinetics and oxidation mechanism of pyrene initiated by hydroxyl radical. A theoretical investigation, Chem. Phys. 528 (2019), 110522.

[69] M.A.M. Mahmoud, A. Shiroudi, M.A. Abdel-Rahman, M.F. Shibl, S. Abdel-Azeim, A.M. El-Nahas, Structures, energetics, and kinetics of H-atom abstraction from methyl propionate by molecular oxygen: ab initio and DFT investigations, Comput. Theor. Chem. 1196 (2021), 113119.

[70] A. Shiroudi, M.A. Abdel-Rahman, A.M. El-Nahas, M. Altarawneh, Atmospheric chemistry of oxazole: the mechanism and kinetic studies on oxidation reaction initiated by OH radicals, New J. Chem. 45 (2021) 2237–2248.

[71] J.C. Keck, Variational theory of chemical reaction rates applied to three-body recombinations, J. Chem. Phys. 32 (1960) 1035–1050.

[72] A. Shiroudi, E. Zahedi, Understanding the kinetics of thermal decomposition of 2,3-epoxy-2,3-dimethylbutane using RRKM theory, RSC Adv. 6 (2016) 91882–91892.

[73] E. Márquez, J.R. Mora, T. Cordova, G. Chuchani, DFT calculations of triethyl and trimethyl orthoacetate elimination kinetics in the gas phase, J. Phys. Chem. A 113 (2009) 2600–2606.

[74] H.S. Johnson, J. Heicklen, Tunneling corrections for unsymmetrical Eckart type potential barriers, J. Phys. Chem. A 66 (1962) 532–533.

[75] J. Troe, Theory of thermal unimolecular reactions at low pressures. II. Strong collision rate constants: applications, J. Chem. Phys. 66 (1977) 4758–4775.

[76] F.M. Mourits, H.A. Rummens, A critical evaluation of Lennard-Jones and stockmayer potential parameters and of some correlation methods, Can. J. Chem. 55 (1977) 3007–3020.

[77] R.J. Kee, F.M. Rupley, J.A. Miller, M.E. Coltrin, J.F. Grcar, E. Meeks, H.K. Moffat, A.E. Lutz, G. Dixon-Lewis, M.D. Smooke, J. Warnatz, G.H. Evans, R.S. Larson, R.E. Mitchell, L.R. Petzold, W.C. Reynolds, M. Caracotsios, W.E. Stewart, P. Glarborg, C. Wang, C.L. McLellan, O. Adigun, W.G. Houf, C.P. Chou, S.F. Miller, P. Ho, P.D. Young, D.J. Young, D.W. Hodgson, M.V. Petrova, K.V. Puduppakkam, CHEMKIN, Reaction Design Inc., San Diego, 2010.

[78] I.M.T. Davidson, C.J.L. Metcalfe, Gas-phase reactions of halogenoalkylsilanes. Part II. 2-Chloroethylethyldichlorosilane, J. Chem. Soc. (1964) 2630–2633.

[79] W. Sun, L. Yang, L. Yu, M. Saeys, Ab initio reaction path analysis for the initial hydrogen abstraction from organic acids by hydroxyl radicals, J. Phys. Chem. A 113 (2009) 7852–7860.

[80] G. Kortüm, W. Vogel, K. Andrussow, Dissociation Constants of Organic Acids in Aqueous Solution, Butterworths, London, 1961.

[81] G.S. Hammond, A correlation of reaction rates, J. Am. Chem. Soc. 77 (1953) 334–338.

[82] N. Agmon, R.D. Levine, Energy, entropy and the reaction coordinate: thermodynamic-like relations in chemical kinetics, Chem. Phys. Lett. 52 (1977) 197–201.

[83] G. Lendvay, Bond orders from ab initio calculations and a test of the principle of bond order conservation, J. Phys. Chem. A 93 (1989) 4422–4429.

[84] K.B. Wiberg, Application of the pople-santry-segal CNDO method to the cyclopropylcarbinyl and cyclobutyl cation and to bicyclobutane, Tetrahedron 24 (1968) 1083–1096.

[85] A.E. Reed, J.E. Carpenter, F. Weinhold, NBO version 3.1, 2003.

[86] A. Moyano, M.A. Periclas, E. Valenti, A theoretical study on the mechanism of the thermal and the acid-catalyzed decarboxylation of 2-oxetanones (β-lactones), J. Org. Chem. 54 (1989) 573–582.

[87] F. Rosas, R.M. Dominguez, M. Tosta, J.R. Mora, E. Marquez, T. Cordova, G. Chuchani, The mechanism of the homogeneous, unimolecular gas-phase elimination kinetic of 1,1-dimethoxycyclohexane: experimental and theoretical studies, J. Phys. Org. Chem. 23 (2010) 743–750.

[88] G. Chuchani, J.A. Hernandez, M. Yepez, M.E. Alonso, Kinetics of the gas-phase elimination of isopropyl α-halo acetates and the taft correlation, Int. J. Chem. Kinet. 9 (1977) 811–818.

[89] T.M. El-Gogary, L.A. Heikal, M.A. Abdel-Rahman, A.M. El-Nahas, First-principle kinetic studies of unimolecular pyrolysis of isopropyl esters as biodiesel surrogates, Theor. Chem. Acc. 140 (2021) 110.

[90] M.A. Abdel-Rahman, A.M. El-Nahas, J.A. Simmie, S. Abdel-Azeem, S.H. El-Demerdash, A.B. El-Meleigy, M.A.M. Mahmoud, A W1 Computational study on the kinetics of pyrolysis of biodiesel model: methyl propanoate, New J. Chem. 45 (2021) 19531–19541.

[91] M.A. Abdel-Rahman, N. Al-Hashimi, M.F. Shibl, K. Yoshizawa, A.M. El-Nahas, Thermochemistry and kinetics of the thermal degradation of 2-methoxyethanol as possible biofuel additives, Sci. Rep. 9 (2019) 4535–4550.

[92] J.S. Al-Otaibi, M.A.M. Mahmoud, A.H. Almuqrin, T.M. El-Gogary, M.A. Abdel-Rahman, A.M. El-Nahas, Ab initio-based kinetics of hydrogen atom abstraction from methyl propionate by H and CH_3 radicals: a biodiesel model, Struct. Chem. 32 (2021) 1857–1872.

[93] J.S. Al-Otaibi, M.A. Abdel-Rahman, A.H. Almuqrin, T.M. El-Gogary, M.A.M. Mahmoud, A.M. El-Nahas, Thermo-kinetic theoretical studies on pyrolysis of dimethoxymethane fuel additive, Fuel 290 (2021), 119970.